



Point set morphological filtering and semantic spatial configuration modeling: Application to microscopic image and bio-structure analysis

Nicolas Loménie ^{a,b,*}, Daniel Racoceanu ^{a,c}

^a CNRS—French National Center for Scientific Research, CNRS UMI IPAL (I2R/A*STAR, NUS, UJF, IT, UPMC), Singapore

^b University Paris Descartes—Sorbonne Paris Cité, France

^c National University of Singapore, Singapore

ARTICLE INFO

Article history:

Received 4 January 2010

Received in revised form

19 December 2011

Accepted 28 January 2012

Available online 14 February 2012

Keywords:

Shape analysis

Mesh analysis

Unorganized point set

Spatial relation modeling

Mathematical morphological operator

Image exploration

Graph representation

Semantic query

Visual reasoning

Digital histopathology

ABSTRACT

High-level spatial relation and configuration modeling issues are gaining momentum in the image analysis and pattern recognition fields. In particular, it is deemed important whenever one needs to mine high-content images or large scale image databases in a more expressive way than a purely statistically one. Continuing previous efforts to incorporate structural analysis by developing specific efficient morphological tools performing on mesh representations like Delaunay triangulations, we propose to formalize spatial relation modeling techniques dedicated to unorganized point sets. We provide an original mesh lattice framework which is more convenient for structural representations of large image data by means of interest point sets and their morphological analysis. The set of designed numerical operators is based on a specific dilation operator that makes it possible to handle concepts like “between” or “left of” over sparse representations of image data such as graphs. Based on this new theoretical framework for reasoning about images, we are able to process high-level queries over large histopathological images, knowing that digitized histopathology is a new challenge in the field of bio-imaging due to the high-content nature and large size of these images.

© 2012 Elsevier Ltd. All rights reserved.

1. Introduction

Shape in computer vision usually refers to either an explicit segmented region over a radiometric image or an implicit feature vector as in Fig. 1. It is less commonly handled as a visual geometrical point set. Yet it has been long the traditional way to define synthetic object models in computer graphics. Recently, representations of virtual models as point sets have started to overtake the mainstream polygonal mesh or spline surface modeling due to both hardware considerations and a few theoretical advances [1].

On the other side of visual computing issues, traditional image analysis is facing all the more challenging issues as the size, resolution and pace of acquisition of images is exponentially growing, in particular in the satellite and medical fields generating huge amount of visual database to be processed. In that perspective, sparse handling of these data as opposed to redundant radiometric traditional coding schemes must be studied [2].

* Corresponding author at: CNRS—French National Center for Scientific Research, CNRS UMI IPAL (I2R/A*STAR, NUS, UJF, IT, UPMC), Singapore.
Tel.: +65 64082548.

E-mail address: lomenie@mi.parisdescartes.fr (N. Loménie).

Concise representations of images by means of structural elements like edges, point sets or graphs of regions are picking up in the computer vision community [3–7] and in particular in medical imaging applications [8–10]. Geometrical representations like point sets for shape or pattern analysis are a means to smooth the way to the efficient handling of large radiometric images: first, geometric features are more stable than radiometric ones and second, as a global representation, they encompass more structural information than local radiometric patches do.

We are ultimately interested in extending usual image analysis tools to geometric representations such as perceptual graphs [11]. Beyond current mainstream works about statistical pattern recognition in the field of image analysis, roughly boiling down to a specific feature extraction step feeding supervised classification algorithms like support vector machines, the research works about structural representations of the image signal is gaining momentum [3,4] even for the recognition of natural categories like horses. Ref. [5] proposed to use contour fragments as descriptors instead of radiometric patches and build a kind of structural codebook composed of the outer object contour fragments associated to their position with regard to the center of the object. Ref. [6] brought a major improvement to the representation by a coding (invariant to scale, translation and rotation) of

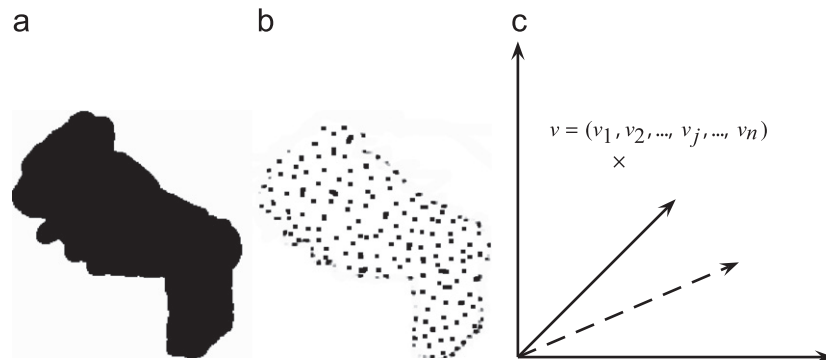


Fig. 1. Shape as (a) a segmented subset of \mathbb{R}^2 ; (b) a point set representation; and (c) a feature vector $v \in \mathbb{R}^n$.

the geometric properties of each group of k adjacent segments (kAS). One key point here is the definition of spatial arrangements of structural elements, and that proved to be useful even for natural images. In addition, this structural modeling is likely to be more resilient to radiometric variations inducing learning biases as well as more expressive for end-user interaction issues and, accordingly, to foster the capabilities of now well-studied and efficient statistical models using radiometric patches for instance [13]. The end-user can indeed leverage spatial relation and configuration modeling to enhance the interactive mining process over high-content images or large scale image databases in a more expressive way than a purely statistically one [12].

In this paper, however, we are focusing on spatial arrangement characterization by morphological considerations. In this perspective, we are considering the issue of high-level spatial relation and configuration representations. A few works have dealt with this issue related to spatial reasoning in images from a structural point of view: that is how to model spatial relations like “between” or “around” in a sound and generic framework. Refs. [14–16] provide good overviews or interesting ways for representing spatial relations in particular in the imprecise and uncertain universe of image analysis. From a more general standpoint, this research work is strongly related to the reemerging paradigm about computing-with-words [17] especially in the field of bioinformatics [18] but first introduced in [19] within the fuzzy sets framework.

While most of the algorithmic solutions to this visual reasoning purpose operate either over usual dense radiometric images or within logical, abstract frameworks like first order logic, we propose here an original, theoretically sound and generic framework to work over sparse representations of visual scenes, such as graphs, in an operational way. This paper continues and in a sense completes the previous efforts for developing morphological tools for the analysis of point sets [20] and extends the seminal ideas about spatial relations modeling over sparse representations presented in [21]. In particular, this paper gives (a) a unified version of the mesh morphological operators, (b) develops the set of spatial relationships modeling capabilities and (c) extends it to algorithmic fuzzy versions within a real bio-imaging application whereby the point set nuclei architecture plays a major role. Even though generic, with straightforward applications to clustering issues in machine or manifold learning [22–24] as illustrated in [25], we chose to closely relate this contribution to a specific application (that we are currently developing in the field of high-content histopathological image exploration and analysis) both for illustration and proof-of-concept purposes. The introduction of structural bio-codes based on the morphological operators makes it possible to categorize various biological configurations of cells. In the following Section 2, we expose the medical context of spatial reasoning from an image analysis point of view with a

few but inspiring related existing works. Section 3 reviews the theoretical operators we designed for point set analysis and in particular the mathematical lattice framework. Then Section 4 presents the innovative contribution to the modeling of high-level linguistic spatial relation modeling over sparse representations of images as point sets. Last, Section 5 illustrates the handling of these spatial relationships within the medical application of interest while Section 6 draws significant theoretical and applicative perspectives of research in particular in the bio-imaging field.

2. Motivation in the bio-imaging context

When describing medical or biological images, it is not rare for high-level spatial descriptions to be involved such as anatomical entities being “close to” or “left of” another one. In particular, a few works deal with anatomical descriptions based on macro image analysis [26–28]. Such qualitative reasoning capabilities should be as much as useful at a microscopic level. For instance, in [29], it is stated that there is suggestive evidence that directed the localization of chromatin loci is one mechanism for regulating gene expression within the nucleus: inactivated chromosomes are predominantly located at the periphery of the nucleus, juxtaposed to the nuclear envelope, observing also an inverse correlation between proximity to the nuclear periphery and gene density. In the case of histo-pathological image analysis, not only the aspect but also the spatial configurations of biological entities are of major importance during the prognosis process. In Fig. 2(a), a sketch classification of spatial cell configurations is drawn for the prognosis of breast cancer from histo-pathological images.

The automatic grading from such histo-pathological images remains a major scientific issue from both the computer and the medical sciences sides. The physicians proceed by tedious, collaborative prognosis sessions involving visual description of Whole Slide Images (WSI) and hardly come to a rigorous consensus. The size of a WSI (around eight gigabytes of image data) constitutes by itself a technological barrier to handle the problem with the help of a computerized system. Any new tool enhancing the capabilities of browsing, focusing, exploring and thus, mining such a huge digitalized image slide is valuable for the pathologists in order to perform the grading from numerical data.

The architecture of breast cancer relies on the spatial distribution of different biological entities such as nuclei, tubular formations or *lumina*, all of them to be detected in the image either by the pathologist or by the algorithm. Entails then a mental process of spatial reasoning about these entities and their organization that is not so much explicit because of the size of the slide. Thus, most grading procedures consist in looking at smaller image frames and scoring visual clues such as the size and the texture

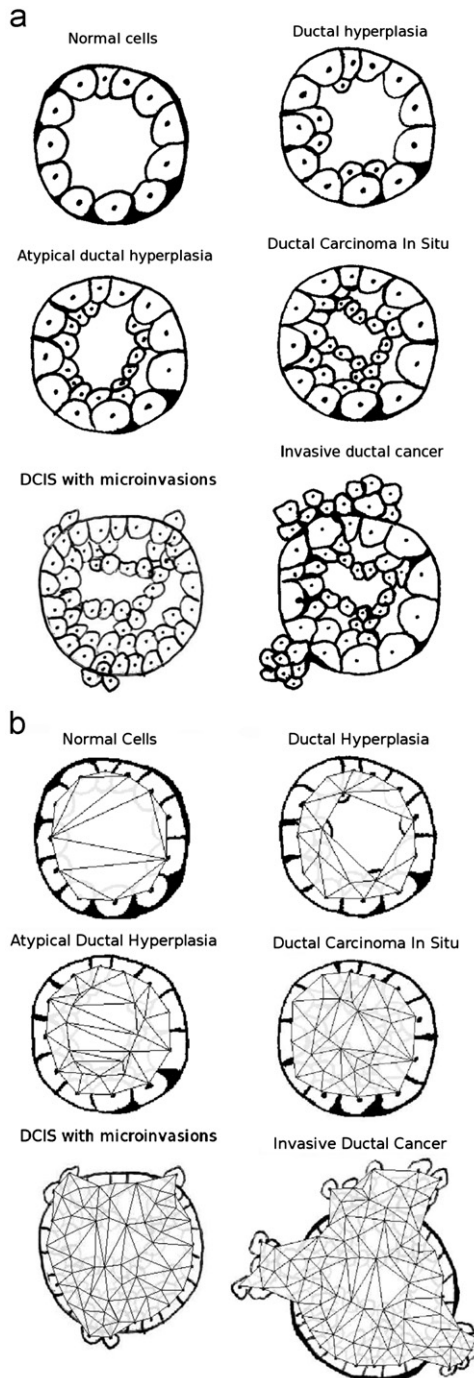


Fig. 2. (a) Theoretical spatial configuration of cells corresponding to various gradings and characteristics of breast cancer—Courtesy of <http://www.breastcancer.org>. (b) Mesh representations with nucleus seeds as vertices of the α -complexes.

of cells as well as the homogeneity of the distribution of these attributes. But, much implicit knowledge involved in that procedure is related to reasoning about spatial relationships. For example, a pathologist will more likely search for mitoses in the periphery of invasive regions. From this statement, any improvement in the way pathologists can perform enriched spatial query in a digitalized slide can improve the quality of the grading. Besides, the basic biological entity is the nucleus which is easier to extract with state-of-the-art image analysis tools than other biological entities. This is the reason why we consider the set of extracted nuclei as a useful, simplified representation of a slide on

which the system can perform efficient spatial query. In addition, this simplified architectural/structural representation is required to handle such an amount of pixel data. Working on a restricted point set representation instead of the radiometric WSI down-sizes this amount of data from around 2.5 billions radiometric color pixels up to 20 000 geometrical 2D points. In [9], the same kind of considerations gave rise to a successful attempt to adapt image processing frameworks (such as Partial Differential Equations based regularization methods) usually acting on radiometric images over a regular grid to unorganized point sets defined within graph representations. From now, the set of nuclei centroids can be seen as a set of geometrical unorganized point sets, that is a minimal structural representation of the architecture of the cell distribution in the tissue.

Thus, we do not work anymore on the regular lattices of radiometric images but on a new irregular lattice dedicated to geometric images. In previous recent works, [20] developed new morphological operators acting on meshes like Delaunay triangulations (see Section 3). The combination of these operators made it possible to build sound and generic spatial relationships operators (see Section 4). We added fuzzy representation capabilities including a new morphological operator acting on meshes and corresponding to the directional dilation as described in [30] for radiometric images. Then, we applied these new operators to the analysis and exploration of histopathological images in order to enhance the cognitive power of interaction between the pathologist and a prototyped virtual microscope (see Section 5). Yet, the designed framework is actually a new generic toolbox to handle structural representations of radiometric images as graphs of interest points. Last, as a proof-of-concept, we developed a Java interface¹ that implements most of the morphological operators acting on Delaunay triangulation described in this paper.

3. Point set and mesh morphological operators

We set up a formal extension to the topological mesh analysis proposed with the concepts of α -objects first exposed in [31,32] to define “what is the shape” of a point set. So far, working on the shape analysis of unorganized point sets, we have developed new morphological operators dealing with mesh structures such as Delaunay triangulations in an efficient algorithmic way [20], w. In the following, our work can be illustrated as both point set analysis operators and mesh structure analysis operators depending on the nature of a specific value ϕ_T . Indeed, based on the same ranking operator max and min as α -objects use it, and directly related to the way mathematical morphology proceeds, we provided a sound theoretical description of these morphological operators. We refer the interested reader to [20,32] to get more details about topological considerations on the data structures and theoretical validation about these new dedicated operators. Nevertheless, for the paper to be self-contained, we give a different presentation (more compact and focused on the lattice framework [34,33]) of these new operators in the following, insofar as, as noted by [35,36], a very few works gave it a try to extend morphology to curved manifolds and to meshes and cell decompositions on curved manifolds [37–41].

3.1. Notations

Topological and geometrical structures. Let S be a point set in \mathbb{R}^2 . Ref. [32] details how to compute the spectrum of α -shapes $S_\alpha(S)$

¹ To test the presented results, a Java application and its source code are available in the public domain at <http://www.sip-crip5.org/lomn/>.

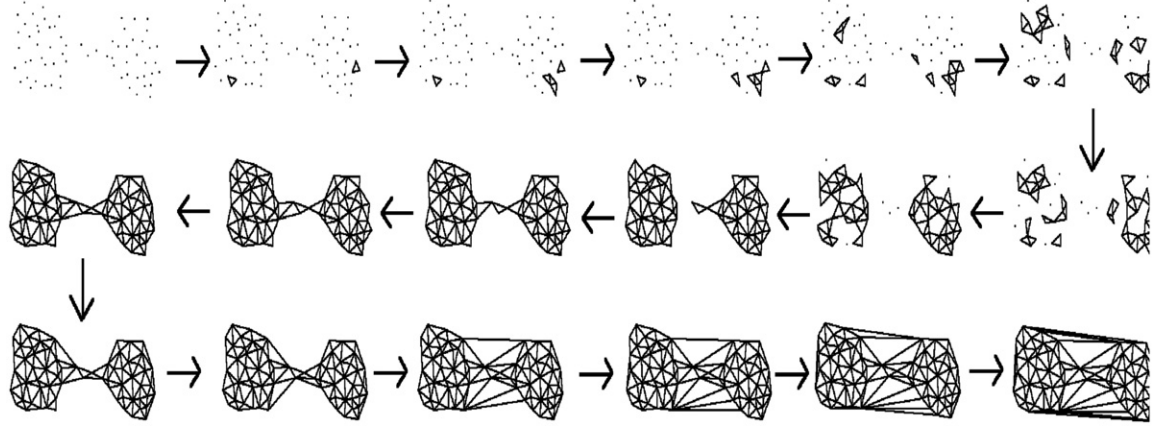


Fig. 3. A spectrum of α -objects derived from the Edelsbrunner's modeling: from S_0 to the meshed convex hull S_∞ of S . For further details about α -complexes, α -shapes, α -hulls definitions, we refer the reader to [20].

for any visual point set in 2D or 3D for any $\alpha \in [0, \infty[$ with: $S_\infty = \text{conv}(S)$, where conv stands for the convex hull, and $S_0 = S$ as limit cases (see Fig. 3 in which the various simplicial α -complexes are depicted).

Let us define k -simplices $\sigma_T = \text{conv}(T)$, $T \subseteq S$ and $|T| = k+1$ for $0 \leq k \leq 2$. Let us remind that the α -object construction relies on the Delaunay triangulation $\text{Del}(S)$ of S and the ϕ_T values associated with any triangle $T \in \text{Del}(S)$ being related to the radius ρ_T of the circumscribe sphere to T in the framework of α -objects.

Lattice structure. For any point set $S \subset \mathbb{R}^2$, $\mathcal{M}(\text{Del})$ is the set of meshes on $\text{Del}(S)$, i.e., the set of mappings from the triangles T in Del to ϕ_T values. As for now, T stands for any triangle in Del . A mesh $M \in \mathcal{M}(\text{Del})$ is defined by $\{(T, \phi)\}_{T \in \text{Del}}$ or equivalently by a mapping $\phi : T \in \text{Del} \rightarrow [0, \infty[$.

From now, we define a complete lattice structure for a point set, within the functional theory frame, called $\mathcal{L} = (\mathcal{M}(\text{Del}), \leq)$, where the partial ordering \leq is defined by: $\forall M_1 \{(T, \phi^1)\}_{T \in \text{Del}} \text{ and } M_2 \{(T, \phi^2)\}_{T \in \text{Del}} \in \mathcal{M}(\text{Del}), M_1 \leq M_2 \iff \forall T \in \text{Del}, \phi_T^1 \leq \phi_T^2$.

3.2. α -Objects and mesh lattices

Depending on the nature of the ϕ_T values, the proposed operators correspond either to an extension of the α -objects concept for point sets or to new mathematical morphological operators acting on meshes. Usually ϕ_T will be in the range $[0, +\infty[$ in the case of intrinsic properties or $[0, 1]$ in the case of extrinsic values. In the case of a ϕ_T value related to intrinsic geometric properties of point set configurations such as the radius of the circumsphere of the σ_T simplices in $\text{Del}(S)$, we can relate our operators to the α -objects concept that gives a set of operators to define and filter the shape of a point set (see Fig. 3). The operator α -bin defined in Eq. (1) makes the connection between our operators and the α -objects-based ones. If $\phi(T)$ is an extrinsic value (such as radiometric values associated to pixels on a regular grid) then our operators constitute new ways to process morphological properties over meshes. The interested reader is referred to [20].

Let us define the binarization operator α -bin as follows:

$$\forall M \in \mathcal{M}(\text{Del}(S)), \quad \alpha\text{-bin}(M) = \{T \in \text{Del}(S) \mid \phi_T > \alpha\} = \text{Del}_\alpha(S) \quad (1)$$

In particular when ϕ_T is the inverse radius of the circumsphere of T , the operator α -bin provides the spectrum of α -region describing the shape of a point set S and we can state that an α -shape(S) is related to a binarization operator acting on spaces whose structure is given by an unorganized point set S , and thus,

$$|\alpha\text{-bin}(M)| = |\text{Del}_\alpha(S)| = |S_{\alpha^{-1}}(S)| \quad (2)$$

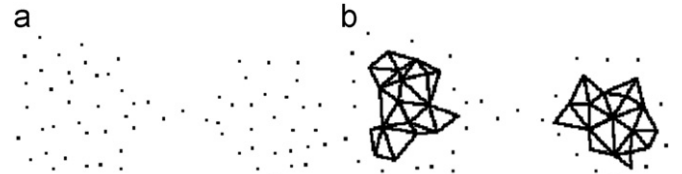


Fig. 4. (a) A point set S in \mathbb{R}^2 and (b) α -eroded(S) for $\alpha = \alpha_{\text{opt}}$.

Based on the lattice structure, the binarization of a point set is defined by

$$\forall S \subset \mathbb{R}^2, \quad \alpha\text{-bin}(S) = \{x \in S \mid \exists T \in \text{Del}(S), x \in T \text{ and } \phi_T > \alpha\} \quad (3)$$

By extension and based on the organic relation between S and $\text{Del}(S)$ in terms of neighborhood and topology, we can write $\alpha\text{-bin}(S) \equiv \alpha\text{-bin}(M)$ where $M = \{T \in \text{Del}(S), 1/\rho_T\}$. In that case, the optimal α value usually set to

$$\alpha_{\text{opt}} = 0.5 * \text{median}_{T \in \text{Del}(S)}(\phi_T) \quad (4)$$

Point set and mesh morphological operators. To define morphological operators, we need to affect to each triangle values e_T and d_T in addition to the measure ϕ_T , defined by

$$\begin{aligned} e_T &= \min\{\phi_{T'} \mid T' \in v(T)\} \\ d_T &= \max\{\phi_{T'} \mid T' \in v(T)\} \end{aligned} \quad (5)$$

where $v(T)$ is the set of all triangles of $\text{Del}(S)$ sharing at least one vertex with the triangle T , that is

$$v(T) = \{T' \in \text{Del} \mid T' \cap T \neq \emptyset\} \quad (6)$$

In our case, $v(T)$ plays the role of a structuring entity (element or graph [37]). We proved in [20] that, with this definition of a structuring entity, the following designed operators are actual mathematical dilation and erosion.

Indeed, in the framework of α -objects, we define the α -eroded of any point set as the reunion of all the triangles of Del_α whose e_T value is superior to α , that is

$$\alpha\text{-eroded}(S) = \{T' \in \text{Del} \mid e_{T'} > \alpha\} \quad (7)$$

as illustrated in Fig. 4.

And in a dual way, the α -dilated of any point set is defined as the reunion of all the triangles of Del_α whose d_T value is superior to α , that is:

$$\alpha\text{-dilated}(S) = \{T' \in \text{Del} \mid d_{T'} > \alpha\} \quad (8)$$

as illustrated in Fig. 5.

Then, in the lattice framework, we define two operators $e(M)$ and $d(M)$ on the complete lattice \mathcal{L} by

$$\forall M \in \mathcal{M}(Del), e(M) = \{T \in Del, e_T\} \quad \text{and} \quad d(M) = \{T \in Del, d_T\} \quad (9)$$

with e_T and d_T defined in Eq. (5).

Last, we state the following:

$$\begin{aligned} \forall M \in \mathcal{M}(Del(S)), \\ \alpha\text{-bin}(e^{\mathcal{L}}(M)) &\equiv \alpha\text{-eroded}(S), \quad \alpha\text{-bin}(d^{\mathcal{L}}(M)) \equiv \alpha\text{-dilated}(S) \end{aligned} \quad (10)$$

showing with Eq. (3) that the designed structures and operators embed the α -object concept in a lattice framework, regardless topological issues due to singular σ_T in the simplicial complex structures. The major interesting point is that with this lattice structure, we inherit all the properties of classical morphology and particularly for the opening and closing filtering operators.

3.3. Mesh morphological filtering: a new tool

We have established so far that a spectrum of filtered shape extracted out of any point set can be computed extending the spectrum of classical α -objects first proposed in [32]. We highlighted the fact that depending on the nature of the ϕ_T values associated to the simplicial complex extracted from S , we get structures directly related to visual shape representation of a point set like in the framework of α -object or we get new operators acting on meshes whose vertices are the sites in S .

From now, we adapt these new tools for a practical use in the case of spatial relationship representation between entities defined over a Delaunay triangulation $Del(S)$ of a point set S .

As for now, ϕ_T values are limited to the interval $[0, 1]$ and related to a notion of visibility of the triangle or of membership to an object of interest within the mesh. Thus, we can define interactively or automatically sub-triangulations of

interest as regions of interest in the meshed image. In the following, we illustrate our results on the histopathological image in Fig. 6(a) and its corresponding underlying meshed nuclei architecture. This image is about 1000×1000 pixels size and each pixel is $0.25 \mu\text{m}$ resolution. The Whole Slide Image contains hundreds of such sample images. In Fig. 6(b), we illustrate the definition of a region of interest over $Del(S)$ by a set of triangles whose ϕ_T values are set to 1 (in white) and others to 0 (no filling color) (Fig. 7).

In that case, the binarization performed by the previously defined operator $\alpha\text{-bin}$ on $Del(S)$ is made by another process either interactively by an end-user or automatically by any image analysis process. We will focus now on operational morphological operators defined on the lattice $\mathcal{L} = (\mathcal{M}(Del), \leq)$ where the mapping ϕ_T is restricted to $[0, 1]$ with a fuzzy interpretation in term of membership function to a region of interest.

Thus, we can define the whole set of operators in a more classical way similar to regular grid formulation used with radiometric images. The structuring entity is the neighborhood $v(T)$ associated to each triangle. The definition of $v(T)$ can vary according to a specific relevant morphological operator (see Section 4). Having proved that the operators designed to obtain these new structures are theoretically sound as mathematical adjunctions, they can provide the whole set of mathematical morphological operators like opening acting on an unorganized point set S or on a mesh M . We can define opening $o(M)$ and closing $c(M)$

$$\forall M \in \mathcal{M}(Del(S)), o(M) = d \circ e(M) \quad \text{and} \quad c(M) = e \circ d(M) \quad (11)$$

where $e(M)$ and $d(M)$ are defined in Eq. (9).

In functional radiometric mathematical morphology, an opening is idempotent but the size of the structuring element is flexible. To adapt the size of the structuring element in the case

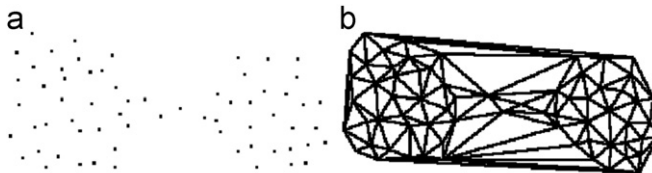


Fig. 5. (a) A point set S in \mathbb{R}^2 and (b) α -dilated(S) for $\alpha = \alpha_{opt}$.

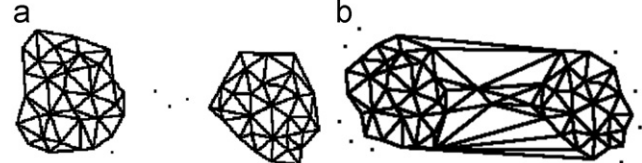


Fig. 7. Illustration of opening and closing for the point set S in \mathbb{R}^2 in Fig. 4; (a) α -open(S) for $\alpha = \alpha_{opt}$ and (b) α -close(S) for $\alpha = \alpha_{opt}$.

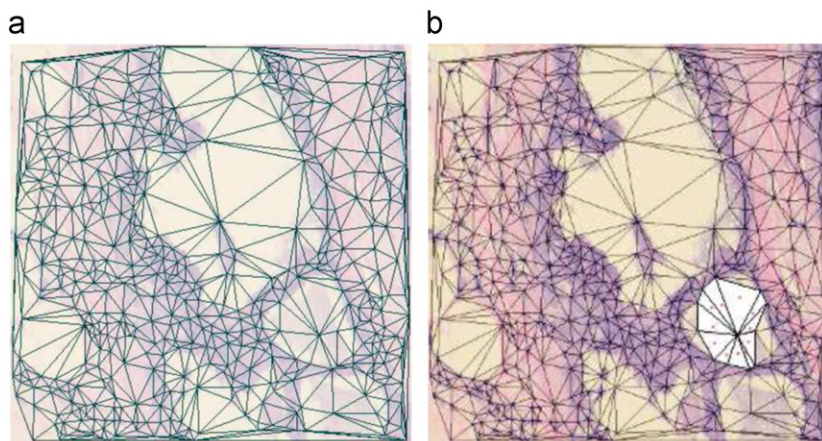


Fig. 6. (a) A real biological image and the underlying nuclei architecture embedded in a Delaunay triangulation $Del(S)$ mesh representation and (b) a crisp region of interest as a sub-triangulation of $Del(S)$: A membership function of 1 is represented by a white triangle and a membership of 0 is represented by a transparent triangle.

of mesh operators, we need to define opening of order n as

$$\forall M \in \mathcal{M}(\text{Del}(S)), \quad o^n(M) = d^n \circ e^n(M) \quad (12)$$

so that

$$\forall n > 1, \quad o^n(M) \neq o(M) \quad (13)$$

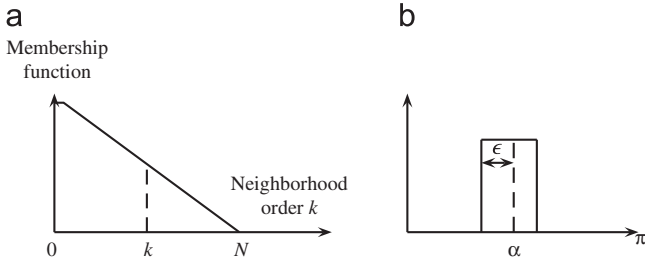


Fig. 8. (a) Discrete membership function along a neighborhood order and (b) crisp angle representation for the directional dilation.

but we still get the idempotent property of the mathematical morphology opening

$$\forall M \in \mathcal{M}(\text{Del}(S)) \text{ and } \forall n \in \mathbb{N}, \quad (d \circ e(M))^n = d \circ e(M) \quad (14)$$

and benefits of all the inherited operators based on the erosion and the involution operators c

$$\forall M \in \mathcal{M}(\text{Del}(S)), \quad M^c = \{T \in \text{Del}, 1 - \phi_T\} \quad (15)$$

Thus, as expected,

$$\forall M \in \mathcal{M}(\text{Del}(S)), \quad e(M) = d(M^c)^c \quad (16)$$

The proof of the theoretical soundness of these operators is directly related to the lattice structure presented in [20] and briefly in the previous subsection. Then, we can deal with new ways of expressing spatial relationships with fuzzy extent over mesh representations like Delaunay triangulations and illustrate how it can benefit the interactive exploration of huge images as the domain of histopathological biopsy images provides.

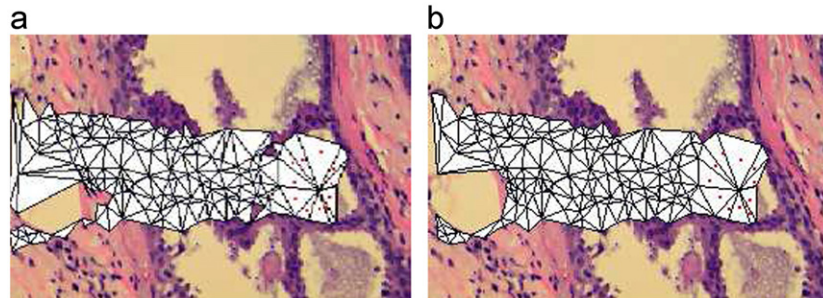


Fig. 9. (a) The left region of the region M_1 in Fig. 6 and (b) the filtered open region left of M_1 with $v_{\text{Iso}} : d_{v_{\text{Iso}}}(\text{Left}_{\text{dil}}(M_1))$.

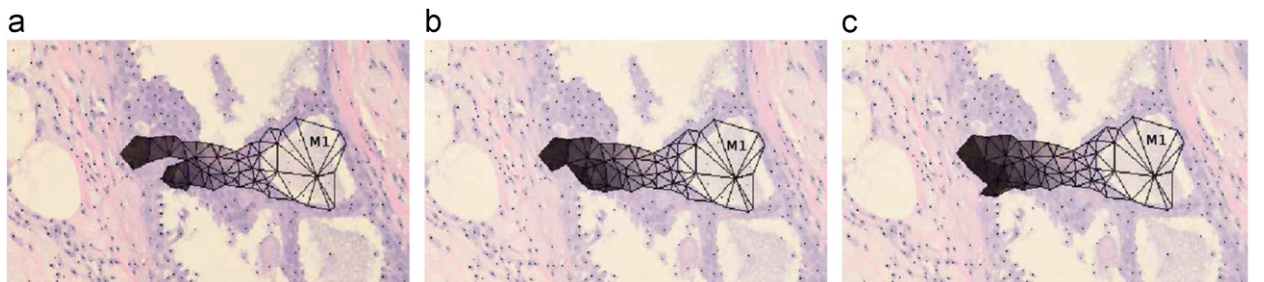


Fig. 10. (a) The fuzzy landscape representing the left region of the region M_1 ; (b) the resulting mesh after an isotropic opening; and (c) the left and near region $\text{Around}_{\text{FuzDil}}(M_1) * o_{v_{\text{Iso}}}(\text{Left}_{\text{dil}}(M_1))$.

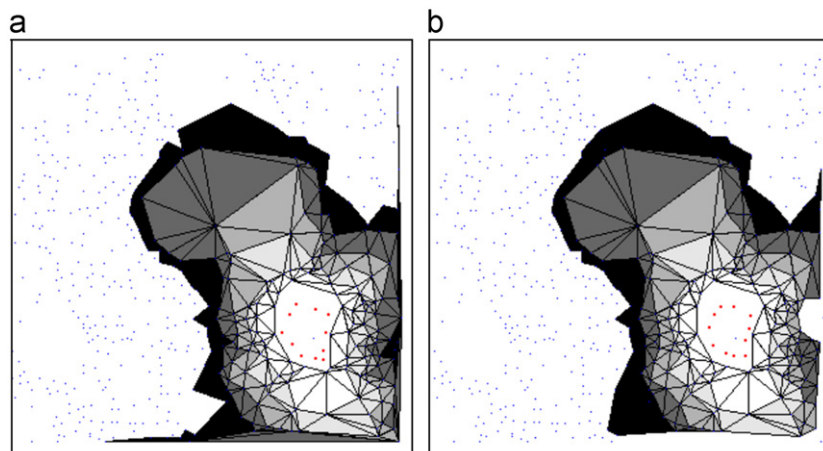


Fig. 11. (a) The fuzzy region 'around M_1 ' and (b) the filtered open region around M_1 .

Extension to fuzzy neighborhood. Let us focus on the dilation operator. A definition of a fuzzy dilation in the functional framework is given by (see [42])

$$D_v(\mu)(x) = \sup_y T(\mu(y), v(x-y)) \quad (17)$$

where μ is the fuzzy set to be dilated, v the structuring element, x and y points of space and T any t -norm (see [44]). Usual t -norms are given by: $T_{\min}(a,b) = a \otimes b = \min(a,b)$ or the Lukasiewicz definition $T_{\text{Luk}}(a,b) = a \otimes b = \max(0, a+b-1) \forall (a,b) \in [0,1]$. With that latter t -norm definition in mind, we propose hereby an algorithmic formulation convenient for the computation of such a fuzzy dilation over an irregular discretized space. Let us define a maximum order of dilation n for the fuzzy dilation. This is related to the shape of a fuzzy structuring element in classical mathematical morphology. We define a fuzzy discrete neighborhood on meshes and a specific t -norm formulation in the case of mesh dilation that makes it possible to compute the fuzzy dilation $d^f(M)$ of a mesh M within the lattice \mathcal{L} using **Algorithm 1**.

Algorithm 1. Fuzzy dilation.

INPUT: a mesh M defined over the lattice \mathcal{L}

for all $i=0$ to $n+1$ do

 for all $T \in \text{Del}$ do

$d_T = 0$;

 end for

 for all $T \in \text{Del}$ do

$\phi_T = d_T$;

 end for

end for

OUTPUT a resulting mesh $d^f(M)$

The fuzzy structuring element or neighborhood is defined in an algorithmic way and can be represented by the discrete membership function along a neighborhood order, as illustrated in Fig. 8(a).

At this point, let us note that defining morphological operators on irregular grids is not as straightforward as often stated [43]. The flexibility of defining versatile structuring elements has not been really handled in a tractable way so far in the world of general graphs [37]. Likewise the definition of sound fuzzy sets over these representations has not been theoretically dealt with. These seminal, practical tools give first insights into the development of morphological operators acting on meshes in 2D as well as in 3D. The next section will focus on semantic spatial relationships modeling based on the designed mesh operators.

4. Mesh morphological operators and spatial relationships

In the field of pure image analysis, few works have dealt with the effective modeling of spatial relations such as “between”, “surround” or “along”. The major difficulty comes from the high level of contextual references associated to the semantic of these linguistic representations of image content. Obviously, inherent issues about accurate, robust segmentation of the regions of interest within the image are part of the difficulties to handle such a tough problem, in comparison with artificial intelligence approaches. For instance, the notion of crisp adjacency that plays a key role within most formal systems dealing with spatial reasoning is error-prone due to imprecise segmentation results. To us, the more interesting modeling results in the field of image processing can be found in [30] for which, besides the use of mathematical morphology operators, a fuzziness representation

framework deals with imprecision and context-dependent numerical implementations of such symbolical descriptions.

Our aim is to apply similar considerations to geometrical representations. Usually, Delaunay triangulations can be associated with the underlying point-of-interests architecture associated with a radiometric image. We state that these simplified representations are more correlated with the semantic of the

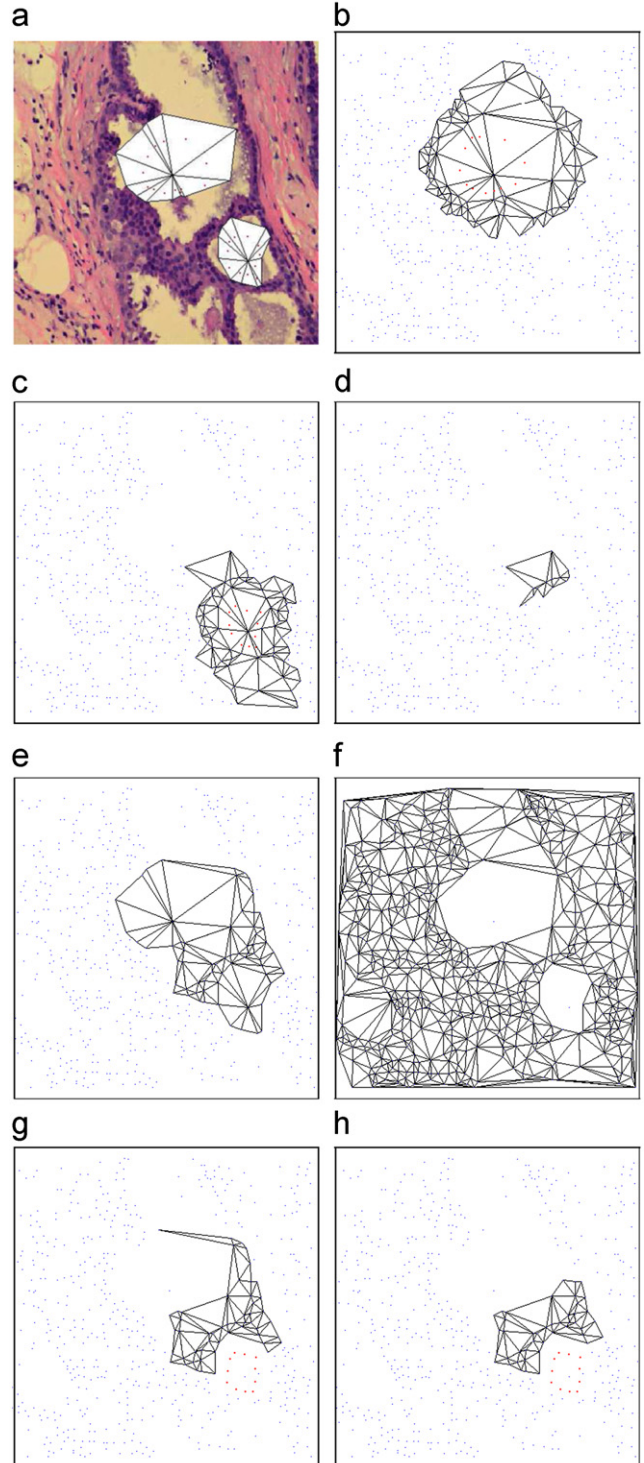


Fig. 12. (a) Two sub-meshes of interest M_1 and M_2 ; (b) the dilated meshes $d^2(M_1)$ and (c) $d^2(M_2)$; (d) their intersection $d^2(M_1) \cap d^2(M_2)$; (e) and the twice dilated of the intersection $d^2[d^2(M_1) \cap d^2(M_2)]$; (f) the complemented mesh $M_1^C \cap M_2^C$; (g) the final output of the between region operator $\beta_{\text{dil}}(M_1, M_2)$ as defined in Eq. (24); and (h) the filtered result after an isotropic opening of $(\beta_{\text{dil}}(M_1, M_2))$.

images and hence consider that spatial relation reasoning on such representations should be closer to the cognitive spatial reasoning processing performed by the pathologists onto histo-pathological images, and more generally by linguistic-based query.

We developed a Java interface as a plugin for the *imageJ* platform to test the proposed operators that implements all the morphological operators acting on Delaunay triangulation described hereby. We added fuzzy representation capabilities included a new morphological operator acting on meshes and corresponding to the directional dilation as described in [30] for radiometric images.

4.1. The directional dilation

The whole set of spatial relation concepts modeling is based on the directional dilation operator defined over regular lattice images. We propose a specific operator for directional dilation over sparse representations such as Delaunay triangulations.

Let α be the directional angle with regard to the horizontal axis of the representation plane. For any mesh $M \in \mathcal{L}$, the definition of the neighborhood $v(T)$ of a mesh triangle T acts as a directional

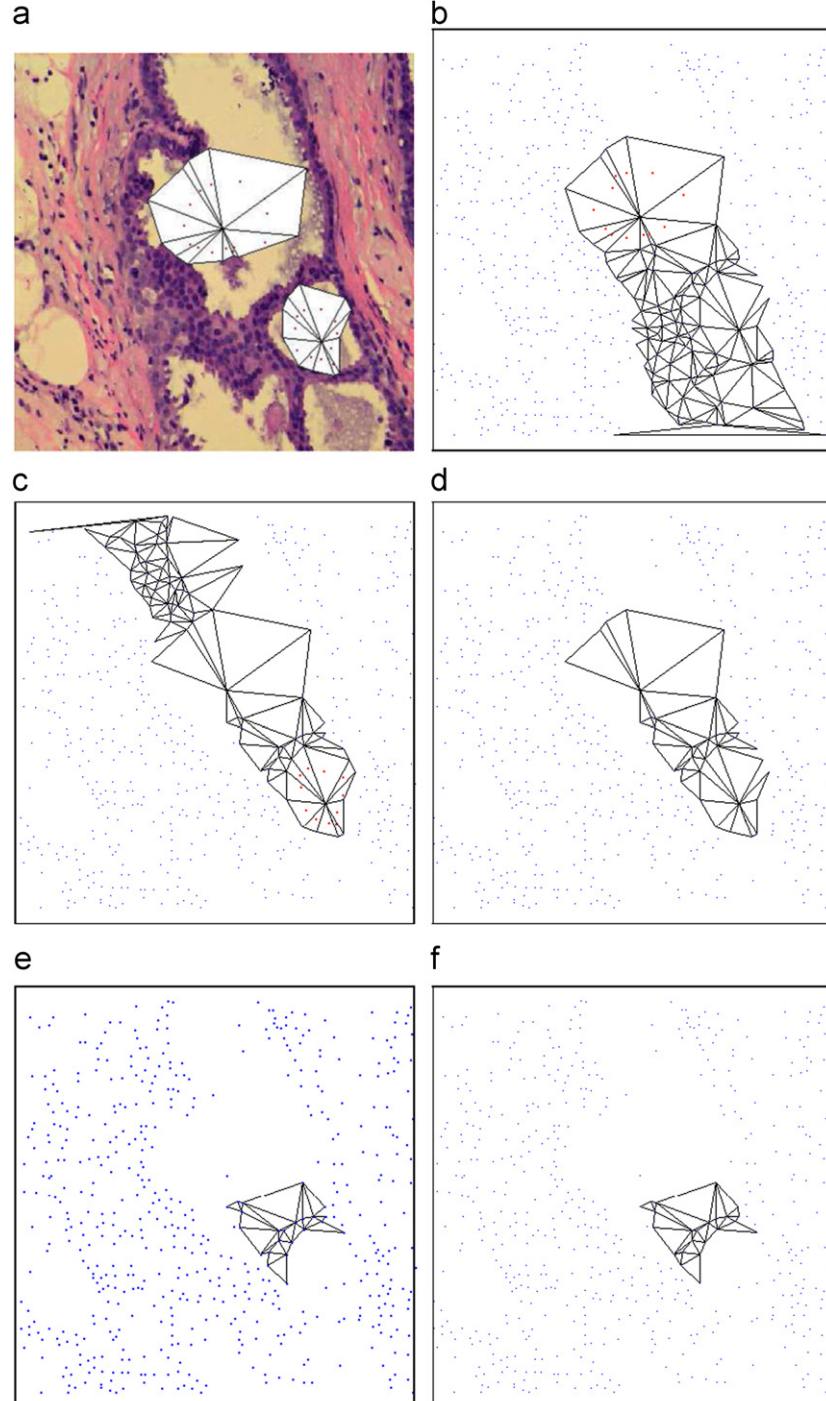


Fig. 13. (a) Two sub-meshes of interest M_1 and M_2 ; (b) the twice dilated meshes $d_\alpha^n(M_1)$ and (c) $d_{\pi+\alpha}^n(M_2)$; (d) the intersection $M_1^C \cap M_2^C$; (e) the region between $\beta_\alpha^1(M_1, M_2)$ as defined in Eq. (24); and (f) after an isotropic opening filtering $o(\beta_\alpha^1(M_1, M_2))$.

structural element of direction α

$$v_\alpha(T) = \{T' \in \text{Del} \mid T' \cap T \neq \emptyset \text{ and } \angle(T, T') < \alpha + \epsilon\} \quad (18)$$

with

$$\angle(T, T') = \angle(\overrightarrow{B_T B_{T'}}, (O \vec{x})) \quad (19)$$

where B_T is the barycenter of the triangle T .

Eq. (18) defines an anisotropic neighborhood referred as v_α , to be put in parallel with the isotropic neighborhood definition $v_{iso}(T) = v(T)$ of Eq. (6), where iso stands for isotropic as opposed to directional and α stands for the angle with the horizontal axis ($O \vec{x}$) and ϵ is the width or tolerance angle of the structuring element (see Fig. 8(b)).

We can define the directional dilation as

$$\forall M \in \mathcal{M}(\text{Del}(S)), \quad d_{\alpha, \epsilon}(M) = d_{v_\alpha}(M) \quad (20)$$

where d_v stands for the computation of d_T values over a specific system of neighborhood v . When ϵ is not written, $\epsilon = \pi/\text{rad}$ and $d_{\alpha, \epsilon} = d_\alpha$.

It is worthwhile being able to define fuzzy appreciations of such qualitative concepts as spatial relations that depend both on the context and on the reference object. This is the reason why we designed a fuzzy version for all the morphological operators acting on meshes following the algorithmic procedure in Algorithm 1. The left fuzzy operator is directly obtained by combining Eq. (20) associated with the directional neighborhood v_α into the algorithmic procedure used to compute d^f .

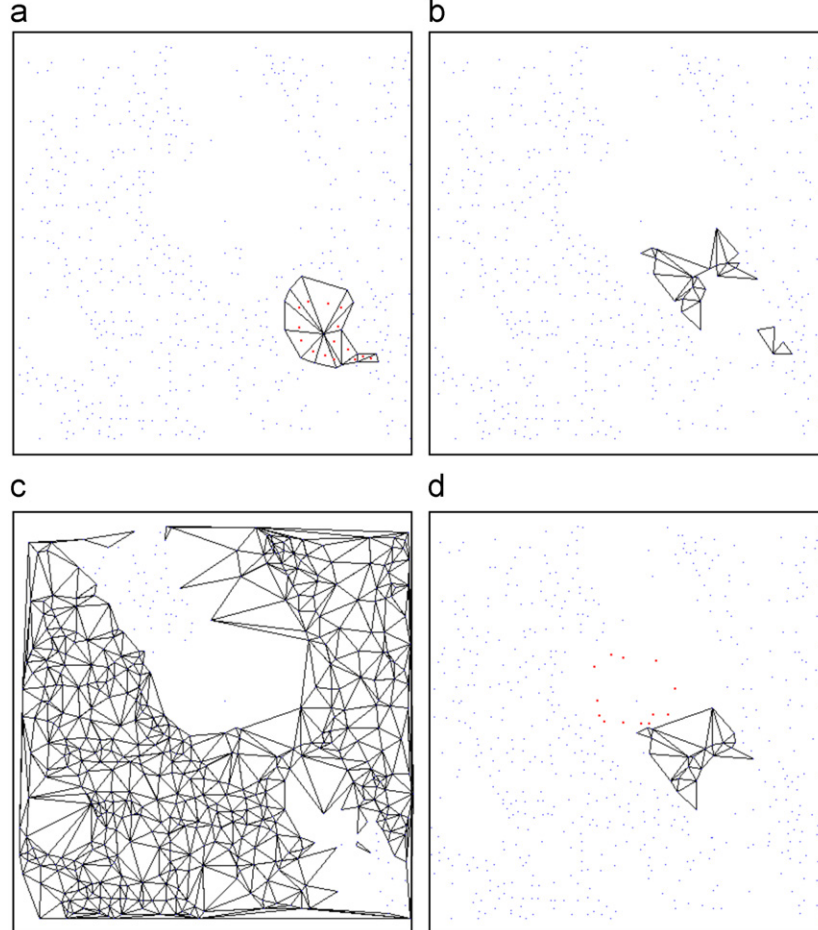


Fig. 14. (a) One non convex sub-mesh of interest M_2 ; (b) result with the second definition $\beta_\alpha^1(M_1, M_2)$; (c) $[d_\alpha(M_1) \cap d_\alpha(M_2)]^C \cap [d_{\pi+\alpha}(M_1) \cap d_{\pi+\alpha}(M_2)]^C$; and (d) result with the third definition $\beta_\alpha^2(M_1, M_2)$.

4.2. The basic relations “left of” and “around”

Directional relations can now be defined. For instance, the absolute directional spatial relation like “left of” is defined as follows:

$$\text{Left}_{dil}(M_1) = d_\pi^n(M_1) \text{ with } n/d_\pi^n(M_1) = d_\pi^{n+1}(M_1) \quad (21)$$

where d^n stands for $d \circ d \circ \dots \circ d$ n times.

Fig. 9 illustrates the region “left of” of the biological *lumina* region M_1 as defined in Fig. 6(b). The region $\text{Left}_{dil}(M_1)$ in Fig. 9(a) corresponds to the left landscape defined over an irregular grid. Due to this irregularity, the output region need to be post-processed with an opening-like mesh filtering or a dilation one. The final filtered region $d_{v_{iso}}(\text{Left}_{dil}(M_1))$ is presented in Fig. 9(b) with holes filled up. In general, any semantic region obtained by the mesh operator needs to be post-processed with an opening-like operator in order to provide compact region to the linguistic queries.

The fuzzy version of the left dilation operator is illustrated in Fig. 10 in which the dilation operator d_π^n is replaced by its algorithmic fuzzy version defined in Algorithm 1 wherein the neighborhood structuring element v is replaced by v_π

$$\text{Left}_{dil}^f(M_1) = d_\pi^f(M_1) \quad (22)$$

Similarly, we can also define a fuzzy spatial relation like “around” as illustrated in Fig. 11:

$$\text{Around}_{fuzDil}(M_1) = d_{v_{iso}}^f(M_1) \quad (23)$$

and its post-processed version with a mesh opening $o(\text{Around}_{fuzDil}(M_1) = d_{v_{iso}}^f(M_1))$ as described respectively in Fig. 11(a) and (b).

4.3. The complex relation “between”

As for now, we can consider the more complex and subjective spatial relation like “between”. We refer the reader to [30] for the thorough presentation of the modeling issues about this very high-level concept, taking into account the extent of the different reference objects. We define here new morphological operators giving the region “between” two spatial mesh entities M_1 and M_2 defined over \mathcal{L} . We refer again to three possible definitions of this relation based on directional dilations, as reviewed in [30]

$$\begin{aligned}\beta_{\text{dil}}(M_1, M_2) &= d^n[d^n(M_1) \cap d^n(M_2)] \cap M_1^C \cap M_2^C \\ \text{with } n &= \inf\{k/d^k(M_1) \cap d^k(M_2) \neq \emptyset\} \\ \beta_\alpha^1(M_1, M_2) &= d_\alpha^n(M_1) \cap d_{\pi+\alpha}^n(M_2) \cap M_1^C \cap M_2^C \\ \beta_\alpha^2(M_1, M_2) &= d_\alpha(M_1) \cap d_{\pi+\alpha}(M_2) \cap M_1^C \cap M_2^C \\ &\cap [d_\alpha(M_1) \cap d_\alpha(M_2)]^C \cap [d_{\pi+\alpha}(M_1) \cap d_{\pi+\alpha}(M_2)]^C\end{aligned}\quad (24)$$

Figs. 12 and 13 illustrate the different steps of the morphological processing of the underlying mesh associated with the studied histopathological image for two regions of interest with the definition β_{dil} and β_α^1 respectively. We based our result on a crisp dilation operator. In case of a fuzzy definition, we replace the mathematical operator d by the algorithmic operator d^ℓ and the \cap operator is a t -norm defined over the mesh lattice by

$$\forall M_1, M_2 \in \mathcal{M}(\text{Del}(S)), \quad M_1 * M_2 = \{T \in \text{Del}(S), \phi_T^1 * \phi_T^2\} \quad (25)$$

with $T(\phi_T^1, \phi_T^2) = \phi_T^1 * \phi_T^2$ a t -norm on the real lattice such as $a * b = \min(a, b)$.

Due to the non-regular pavage of the underlying topological space, a post-filtering step by an isotropic opening filter is

required to obtain coherent results (see Fig. 12(g)). If the second region of interest is not convex, as illustrated in Fig. 14, the third definition gives better results removing parts in the concavity.

In general, the choice of the angle α should incorporate much information about the extent of the different objects of reference. In this study, we choose the average angle between pairs of respective triangles $T_1 \in M_1$ and $T_2 \in M_2$. Note also that the tolerance angle is set quite large to 22.5° to smooth the results to the irregular pavage of the 2D space (see Section 5 for more discussion about that specific issue).

4.4. High-level query

With the specific morphological framework defined over meshes, we are able to define high-level semantic queries over a mesh representation of objects of interest by combining different operators via t -norm when conjunctions of properties occur or t -conorm (like the max operator that stands also for the set operator \cup) when disjunctions of properties occur [44]. For example, we can express the query

Show me the region near and left the region M_1 .

by means of the following operator:

$$\text{NearLeft}(M_1) = \text{Around}_{\text{fuzDil}}(M_1) * \text{o}_{v_{\text{iso}}}(\text{Left}_{\text{dil}}(M_1)) \quad (26)$$

with $*$ a t -norm defined over the mesh lattice (see Eq. (25)). Fig. 10(c) illustrates the result on the biological image.

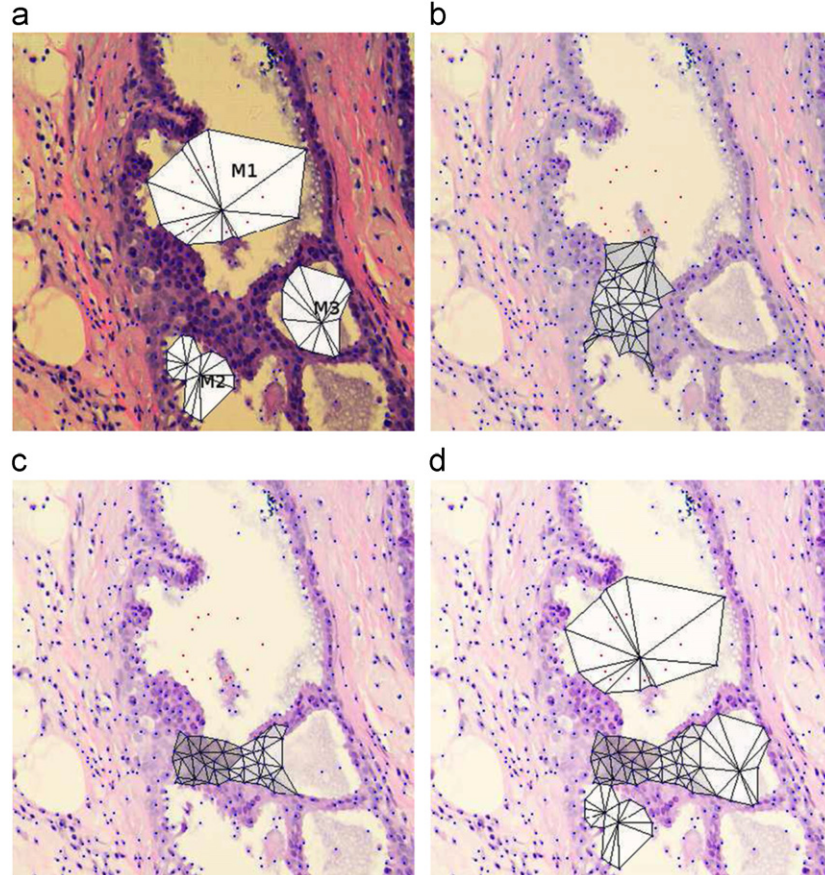


Fig. 15. (a) Three meshed regions of interest M_1, M_2 and M_3 ; (b) the region between M_1 and M_2 $\beta_\alpha^1(M_1, M_2)$; (c) $\beta_\alpha^1(\beta_\gamma^1(M_1, M_2), M_3)$; and (d) with the three regions superimposed in transparency.

5. Applications and discussion

All these functionalities are useful whereby one needs to reason about spatial entities corresponding to unorganized point sets as in the case of nuclei extracted from medical images (see [10] for interesting statistical analysis of nuclei architecture structures embedded in a mesh representation for breast cancer diagnosis). Seminal works tried to apply similar structural analysis of tissue images based on Delaunay graphs representations few years ago [45,46] but have not been pushed forward so far. This is what we propose in the following, in particular for digitized histopathology image analysis which is a brand new

challenge in the field of bio-imaging as digital mammograms used to be over the last two decades.

5.1. Spatial relation concepts

As for now, we can answer the two types of questions raised by spatial reasoning:

- Which is the region of space corresponding to a spatial query about a reference object M_i ? And, if necessary, what is the fuzzy mesh description of this region?
- To which degree an object O belongs to that region?

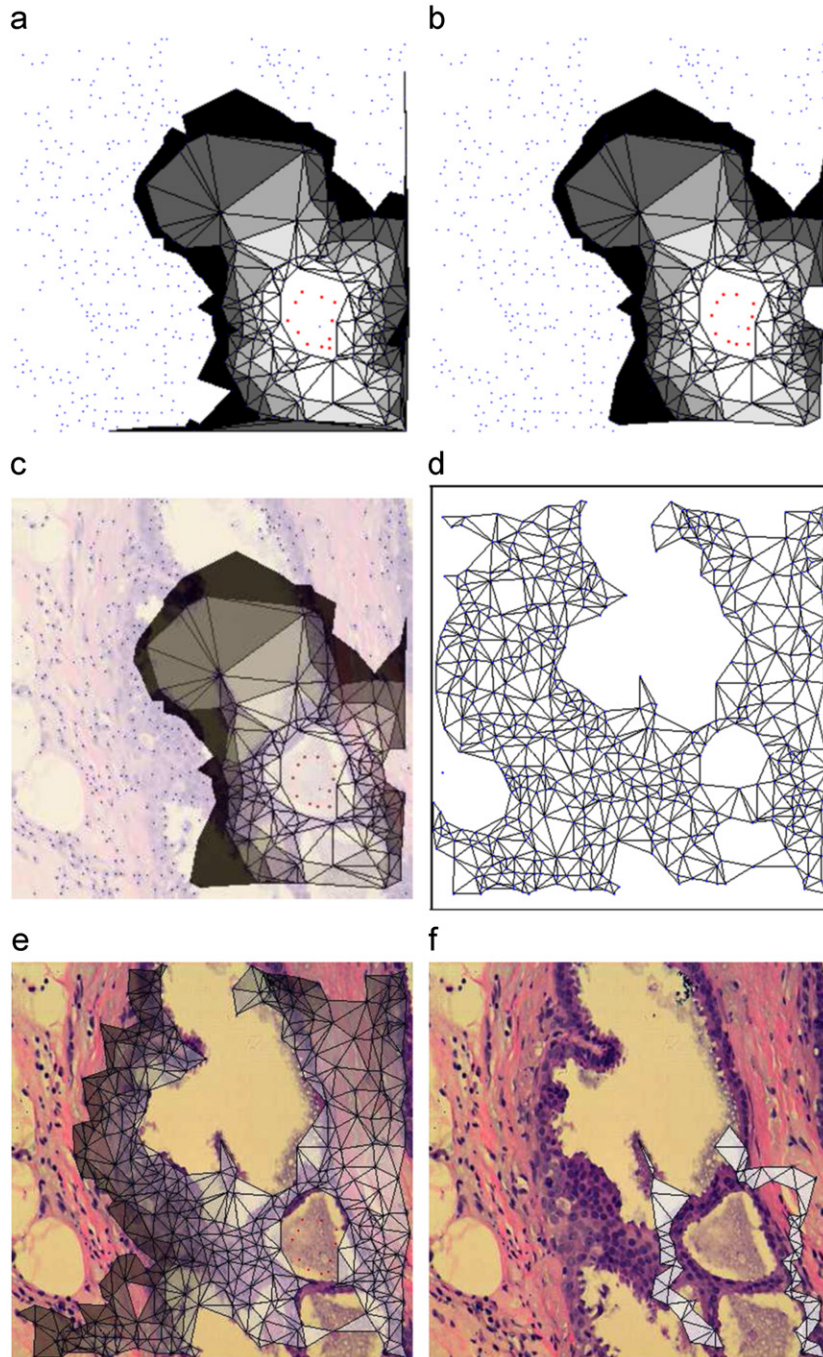


Fig. 16. (a) Fuzzy meshed region M_a “around” the central region M_3 ; (b) the opening of this region $o(M_a)$; (c) in transparency over the biological image; (d) the binarized Delaunay triangulation $M_b = \alpha\text{-bin}(Del(S))$; (e) $M_f = M_b \cap o(M_a)$; and (f) $\alpha\text{-bin}(ProximityLevelSet \cap M_f)$.

In comparison to the seminal works in [30], we can answer these questions with specific tools over a mesh representation. Our operators work on irregular pavages of the space corresponding to the informative structural part within the image and not on the classical regular pavages over radiometric images. We remind the reader the importance of such a simplified representation in the case of high content image or large image data like new satellite or microscopic imaging devices provide from now on in a breakthrough way. These representations should be more efficient than classical radiometric, redundant by nature, images and their related processing algorithms not tractable for now over large amount of data due to computational and storage constraints.

In the previous section, we illustrated with numerous examples the numerical nature of answers our operators “around”, “left of”, and “between” can reach to deal with the first type of questions, possibly with a fuzzy description of these meshed resulting regions. In this section, we go further in the description of the operator outcomes from the end-user interaction point of view ending up with a discussion about the efficiency of such a sparse modeling of spatial relations. Fig. 15 illustrates the regions corresponding to the fuzzy version of the *Between* operator $\beta_\alpha^f(M_1, M_2)$ for the regions M_1 and M_2 and then the region between M_1 , M_2 and M_3 can be obtained by the combination of such operators such as

$$\text{Between}(M_1, M_2, M_3) = \bigcup_{(i,j,k) \in \sigma(1,2,3)} \beta_\alpha^f(\beta_\gamma^f(M_i, M_j), M_k) \quad (27)$$

as Fig. 15(c) and (d) illustrates it for $\beta_\alpha^f(\beta_\gamma^f(M_1, M_2), M_3)$ and with σ the cyclic permutation operator.

In Fig. 16, we illustrate a level set for the fuzzy operator “around” for the inner region of interest M_3 . The topology and density underlying the biological image is taken into account in contrast to the usual notion of iso-density distance usually used for radiometric morphological image operators.

That simplified representation based on the natural architecture of the image is of major importance with the new imaging devices providing such high-content, large image data at very high rate. For the sake of illustration, in our histopathological application, Table 1 gives an idea of the amount of data to be processed by either the clinician or the numerical system. Then, Fig. 17 illustrates the level of details depending on the acquisition resolution. Note that the images at each of the listed resolution must be stored for clinical and virtual microscopy purposes. The sample in Fig. 17 is a 1024×1024 pixels sample image at a resolution $40 \times$ out of over two thousands such samples tiling the global image slide.

5.2. Structural bio-codes

These morphological operators can be applied as it is to perform structural analyses of different nuclei architectures of breast cancers. In Fig. 18, the classification of sketched cases of various types of breast cancer architectures can be achieved by morphological and topological analyses of the underlying meshes.

Table 1
Histopathological images data.

Magnification	Size (pixels)	Size (bytes)
1 ×	1018×768	3.05 Mo
10 ×	3664×2763	39.54 Mo
20 ×	$14\,657 \times 11\,054$	632.48 Mo
40 ×	$58\,630 \times 44\,216$	7.77 Go

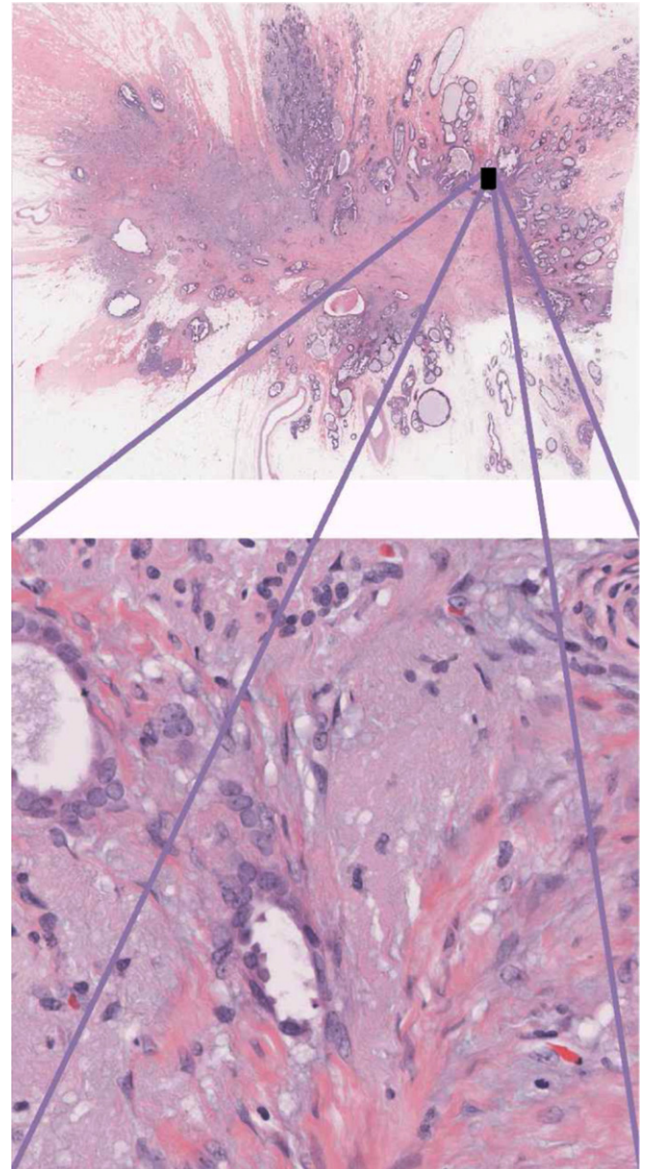


Fig. 17. Top: WSI at resolution/magnification 1 ×. Bottom: sample image at resolution $40 \times$ out of over 2000 samples tiling the WSI.

For the sake of illustration, we present below how with very basic morphological operators on such kinds of geometrical architectures we can discriminate at a high-level of description between various kinds of breast cancer configurations. In Fig. 18, a morphological analysis based on both the α -complex and an opening filtering of the underlying Delaunay triangulations Del_α of the set of nuclei centroids can lead to an effective discrimination of these differently graded histo-pathological breast cancer drawings.

Referring to the last row in Fig. 18 related to Invasive Ductal Cancer cases, the image processing line proceeds as follows: first in (a) an optimal simplicial complex representation $\text{Del}_{\alpha_{\text{opt}}}$ of the nuclei architecture is computed and can be regarded as the optimal α -complex of minimal surface and containing all the nuclear vertices; then, in (b) the opening of order two is computed: $\text{o}^2(\text{Del}_{\alpha_{\text{opt}}})$ that filters out the outgrowths in the invasive cases; last, in (c) the final simplicial complex $\text{Del}_{\alpha_{\text{opt}}} - \text{o}^2(\text{Del}_{\alpha_{\text{opt}}})$ acts as a top-hat morphological filter extracting the filtered outgrowths proper to the

invasive case. This processing line acts as a structural filtering independently of the size, orientation, scale of the structure and performs a high-level analysis of the various cases to be detected where most statistically filters will fail to model the high variability of these structures. In addition no learning phase is necessary which is always a bottleneck in the case of medical image database.

The categorization is based on the comparison of structural features such as the number of connected components or the Euler characteristics related to the topology of the mesh and in particular to the number of holes or connected components in the

structure (see Table 2). For instance, the Euler number EN of a surface is easily computed from the mesh representation as $EN = F - E + V$ where F is the number of faces, E the number of edges and V the number of vertices. Note that this number can be related to the number of connected components minus the number of holes.

In particular, the Ductal Carcinoma In Situ (DCIS), rather difficult to discriminate automatically by statistical means due to its highly versatile structure in shape and size, is characterized by a certain topological and morphological stability to opening

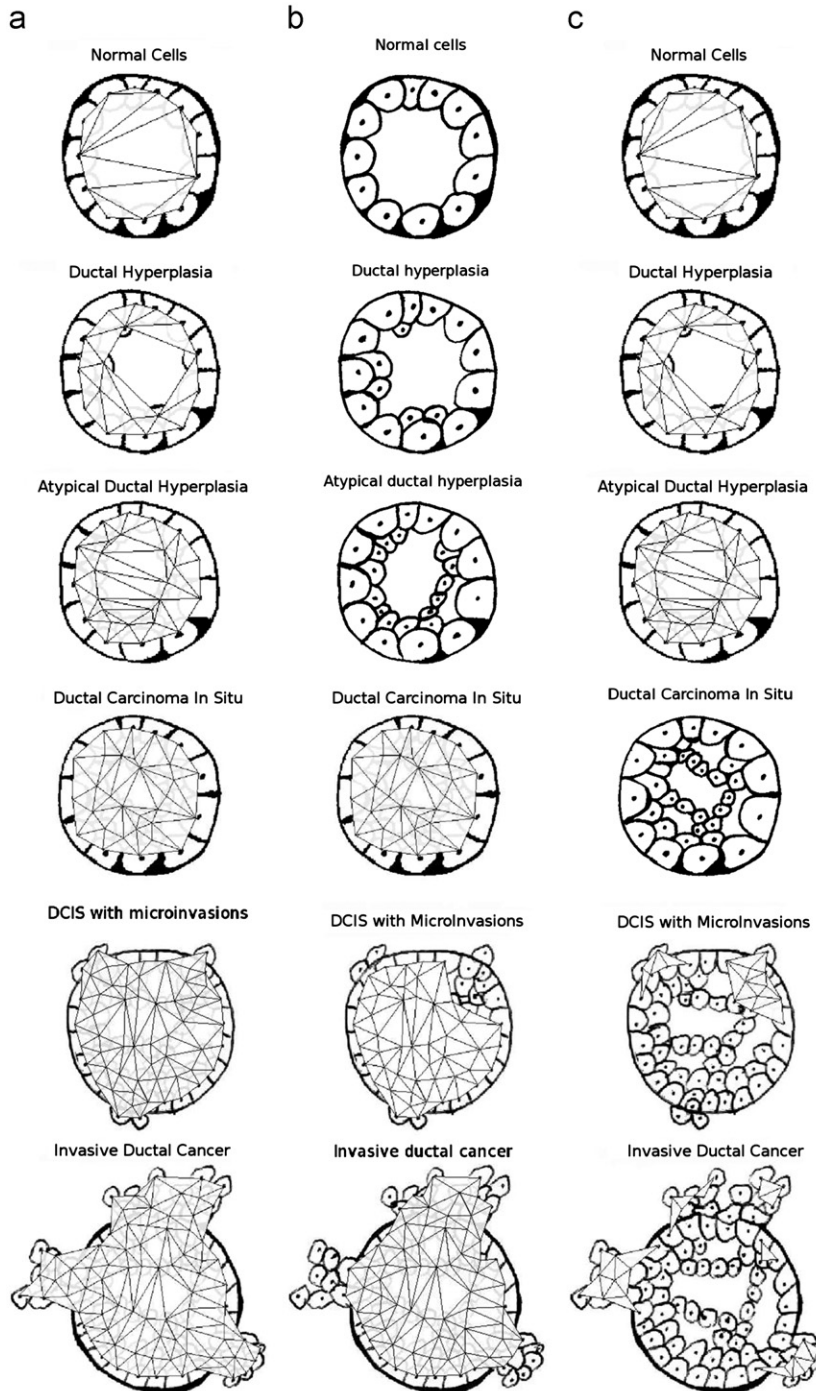


Fig. 18. The nuclei architecture and on the left (a) $Del_{z_{opt}}$ representation; (b) in the middle, opening of order two $o^2(Del_{z_{opt}})$ as an opening based morphological filtering; and (c) at right, the difference between $Del_{z_{opt}}$ and $o^2(Del_{z_{opt}})$. Combining topological and morphological measures such as the number of connected components, the Euler number, the median face size between these various representations makes it possible to discriminate between the various levels of pathological spatial organizations.

Table 2

Geometric criteria to discriminate between various cancer types computed on $M_1 - o^2(M_1)$ (see Fig. 18(c), right column). A median size of 0 refers to small size and of 1 to large size. EN, CC and MS respectively stand for Euler number, number of connected components and median size of the triangles. Their concatenation provides a digital structural coding of the observed bio-structures.

Cancer type	EN	CC	MS
Normal cells	1	1	1
Ductal hyperplasia	0	1	0
Atypical ductal	1	1	0
Ductal Carcinoma In Situ (DCIS)	0	0	0
DCIS with micro-invasions	2	2	0
Invasive	5	5	0

Table 3

Two structural bio-codings of various breast cancer based on the nuclei organization analysis. The bio-code BC_1 is the concatenation of the EN, CC and MS value as extracted in Table 2. The bio-code BC_2 is based on the Euler number computed over the three mesh representations inferred in Fig. 18.

Cancer type	BC_1	BC_2
Normal cells	111	101
Ductal hyperplasia	010	000
Atypical ductal	110	101
DCIS	000	110
DCIS-MI	220	112
Invasive ductal	550	115

filtering ($EN=CC=MS$) in comparison to the other cancer types in Table 2. Interestingly, the normal cells and the DCIS share the stability property through the various morphological filtering. As a matter of fact, DCIS is not considered as a malignant configuration but much more as a pre-malignant one. Also, the invasive and the micro-invasive cases can be discriminated by a thorough analysis of the third column exhibiting more connected components for the invasive case.

Table 3 presents two structural bio-codings of the breast cancer typology based on the nuclei organization analysis within a tissue. The bio-code BC_1 corresponds to the concatenation of the EN, CC and MS values computed over the last column simplicial representation ($identity - o^2(Del_{z_{opt}})$) in Fig. 18 and is detailed in Table 2. The bio-code BC_2 encodes the concatenation of the EN values over the three mesh representations computed in Fig. 18 for each kind of configuration.

Referring to the last row of Fig. 18, the bio-code BC_1 is computed over the last column representation in Fig. 18(c) combining the Euler number $EN=5$, the number of connected components $CC=5$ and the median size of the triangles $MS=0$ standing for small triangles, providing the digital bio-code $BC_1(\text{Invasive Ductal Cancer})='550'$. The code 5 is not a fixed one but will definitely be superior to two for invasive cases. The bio-code BC_2 is computed over the simplicial representations of Fig. 18(a)–(c) by combining the three corresponding Euler numbers and providing the bio-code $BC_2(\text{Invasive Ductal Cancer})='115'$. Discriminating between the six ductal breast cancers in Fig. 18 can be performed based on the structural bio-codes as illustrated in Fig. 19 with various zones in the cube representation corresponding to the various cases.

Experiments on real images have been carried out and showed that structural and morphological criteria involved in automatic procedures provide efficient way to discriminate such spatial configurations as compared with statistical criteria. In Fig. 20, we discriminate between tubule formation and DCIS configuration

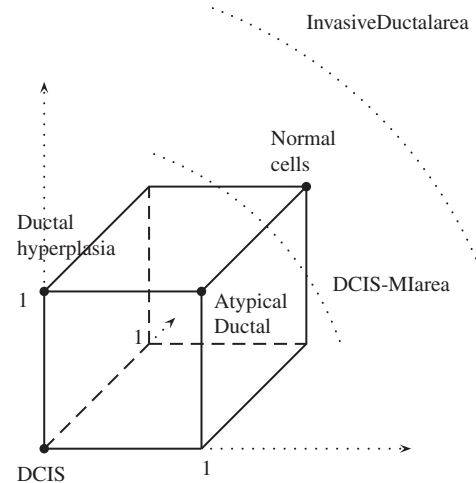


Fig. 19. Repartition of the six various breast cancer cases of Fig. 18 over the three dimensional bio-code cube.

images based on the structural analysis described in Fig. 18. The tubule formation corresponds to the normal cell configuration except that it is not a real duct. It is quite a common natural organization of cells in the tissue. The structural bio-code as referenced in Table 3 is respectively 111 and 000 for the tubular formation and the DCIS configuration. Basically, a dense representation of tubular formations corresponding to a 000 bio-code is a clue for a healthy breast tissue in histopathology and corresponds to the bio-code of a normal cell configuration.

This experiment is carried out in collaboration with domain experts at Hospital La Pitié-Salpêtrière, Paris, France. They annotated Whole Slide Images in terms of objects of interest such as mitosis, cell, invasive area, tubule, DCIS, etc. They acknowledged the dramatic need for them to enter the digital area as mammography did a couple of decades ago. The categorization tool has definitely been proved to be useful at least to focus on regions of interest over the huge amount of high-content data carried by a digital WSI. Both the grading process and the telediagnosis objective should benefit from this new ways of dealing with such data.

5.3. Semantic concepts

From a human-computer interface point of view, Fig. 21 illustrates how the proposed morphological operators are benefiting the end-user (physician or automatic microscope) to focus on regions of interest corresponding to potential *invasive areas* for breast cancer prognosis either in diagnosis or image acquisition mode. The resulting mesh is obtained as $o^2(Del_z(S)) \cap Del_z(S)$. The point sites in Fig. 21(b) are obtained by a basic image analysis procedure combining wavelet analysis, binarization and sampling on a 3072×3072 pixels sub-image taken out of the Whole Slide Image at resolution $40 \times$ whose global size is over two thousands times bigger. Fig. 21(a) corresponds to the Delaunay triangulation of the cell architecture $Del(S)$ and Fig. 21(a) is the result of the point set binarization Del_{opt} . The resulting filtered mesh $o^2(Del_z(S)) \cap Del_z(S)$ focuses on the aggregated cells clue for invasive areas (see Fig. 21(d)). Being able to focus on these zones for the while exploring the WSI enhances the efficiency of diagnosis for the pathologists.

Furthermore, by setting the parameter ϕ_T to a measure related to the size of triangles rather than a measure of the shape as the circumsphere radius characterizes, Fig. 22 illustrates how, with

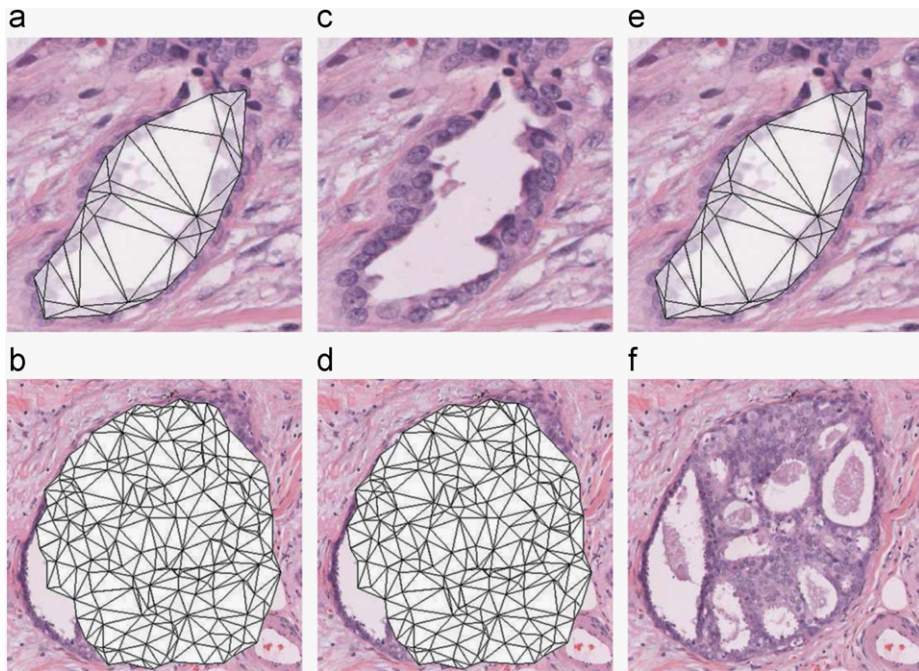


Fig. 20. (a) From left to right: a $\text{Del}_{z_{\text{opt}}}$ representation of a tubular bio-structure, the opening of order two $o^2(\text{Del}_{z_{\text{opt}}})$ and the difference mesh $\text{Del}_{z_{\text{opt}}} - o^2(\text{Del}_{z_{\text{opt}}})$; (b) from left to right: a $\text{Del}_{z_{\text{opt}}}$ representation of a DCIS bio-structure, the opening of order two $o^2(\text{Del}_{z_{\text{opt}}})$ and the difference mesh $\text{Del}_{z_{\text{opt}}} - o^2(\text{Del}_{z_{\text{opt}}})$. These two bio-structures are respectively encoded into the two structural bio-codes 111 and 000 as referenced in Table 2.

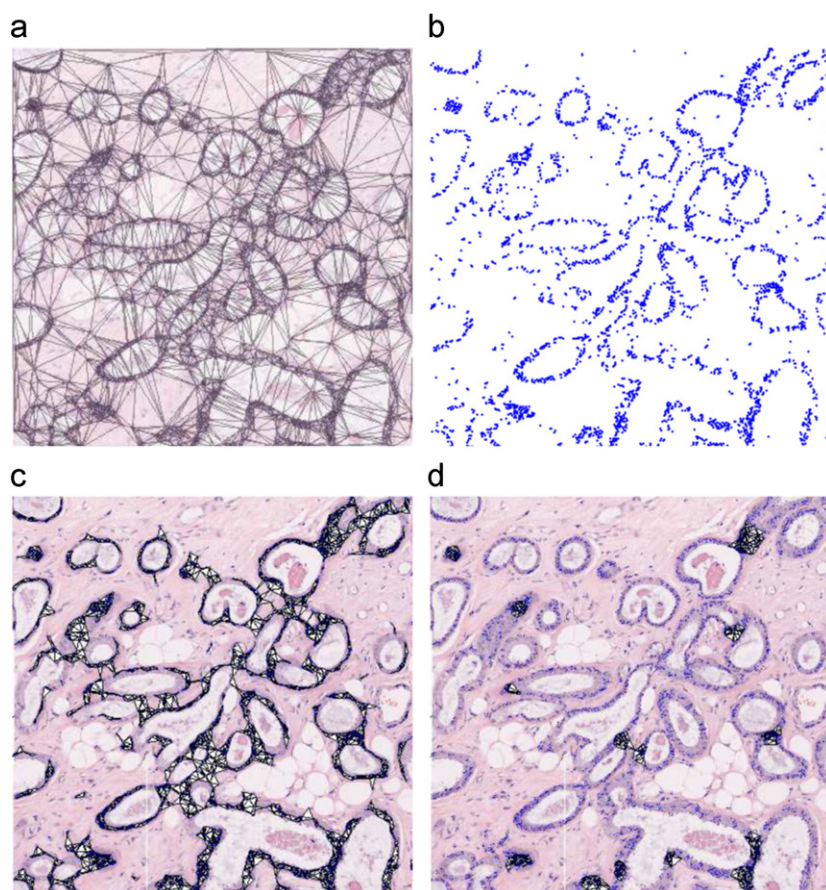


Fig. 21. (a) 3072 × 3072 pixels size sub-image of a whole slide histopathological image; (b) the corresponding site points S ; (c) $\text{Del}_z(S)$; and (d) focusing on regions of interest $o^2(\text{Del}_z(S)) \cap \text{Del}_z(S)$ corresponding to potential invasive areas over which to focus either for the image acquisition or the diagnosis process.

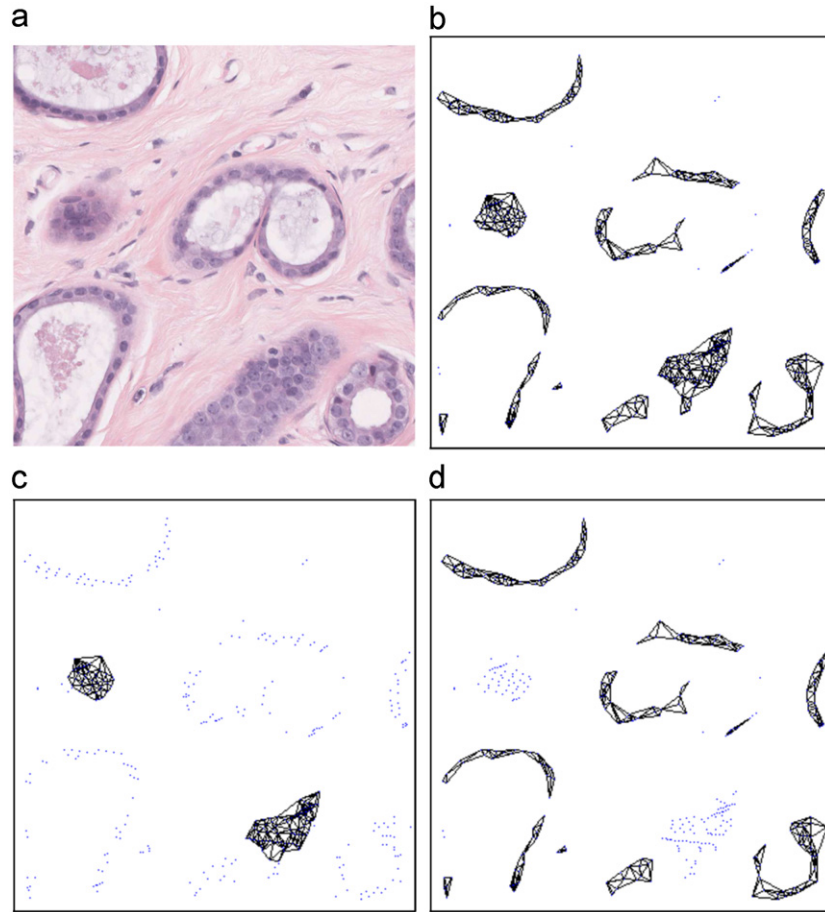


Fig. 22. (a) 1024×1024 pixels size sub-image of a histopathological WSI; (b) $\text{Del}_z(S)$; (c) focusing on DCIS alike areas with the $\sigma^2(\text{Del}_z(S))$ mesh filtering; and (d) focusing on normal cells areas with the $\text{Del}_z(S) \cap (\sigma^2(\text{Del}_z(S)) \cap \text{Del}_z(S))^c$ mesh filtering operator.

minimal interactions, it is possible to decompose the biological images of size 1024×1024 (top left quadrant of the previous image in Fig. 21) into meaningful biological elements like Ductal Carcinoma In Situ alike or normal cells by means of morphological operators. The size measure is defined by $\max(AB, AC, BC)$ where A, B, C are the three vertices of the triangle T . Fig. 22(b) corresponds to the point set binarization providing Del_{opt} . Then, Fig. 22(c) corresponds to the opening filtering of Del_{opt} and focuses on the DCIS-like structure (see Fig. 20(b)). The complemented structure in Fig. 22(d) focuses on normal cell configurations like the tubular one in Fig. 20(a).

Referring to the basic spatial relations “left of” or “around” as defined in Section 4.2, a know-how rule used by pathologists for the visual exploration of histopathological images consists in looking for invasive cancer areas specifically around the nerve structures or mitoses at the periphery of the invasive areas. An automatic platform fully-fledged with our spatial reasoning tools is then able to implement this kind of high-level visual query in a very formal way.

Last, by nature, this set of techniques is quite resilient to low-level image extraction artifacts as illustrated in Fig. 23. In this experiment, only the epithelial cells are detected in Fig. 23(a) and some cell artifacts are detected in Fig. 23(d). This kind of noise is inherent to the low-level cell detection algorithms even though the staining of the cell nuclei makes the cell detection the more robust of the image analysis issues in histopathology [47]. The morphological analysis of the point set is robust to this shape noise for the detection of *in situ* cases as illustrated in

Fig. 23(e) and (f) corresponding to the opening filtered Del_{opt} structures of Fig. 23(c) and (d). Being able to handle shape noise when statistic filtering usually fails at it (unless a huge learning database is available) is one of the highlights of mathematical morphology.

6. Conclusion

To sum up, based on original mathematical morphological filters dedicated to unorganized point sets, we developed new generic operators to perform structural analysis of images via an architectural representation as mesh of interest points for instance. In particular, a new way for handling spatial relation queries has been proposed and illustrations over histopathological images proved the usefulness of this new framework to interactively explore huge images. Beyond the applicative aspect, these operators have been proved to be theoretically sound from the mathematical lattice framework side. Accordingly, these tools open new ways to anchor high-level semantic and spatial relation concepts in the field of image analysis.

As a perspective related to an emerging topic discussed in [48,49], an extension of the morphological operators to a lattice of simplicial complexes including the edges and the vertices of the meshing structures should raise interesting new mathematical theoretical issues. Such powerful computerized representations aiming at fine topological analysis should be helpful for the understanding of biological processes and spatial organizations.

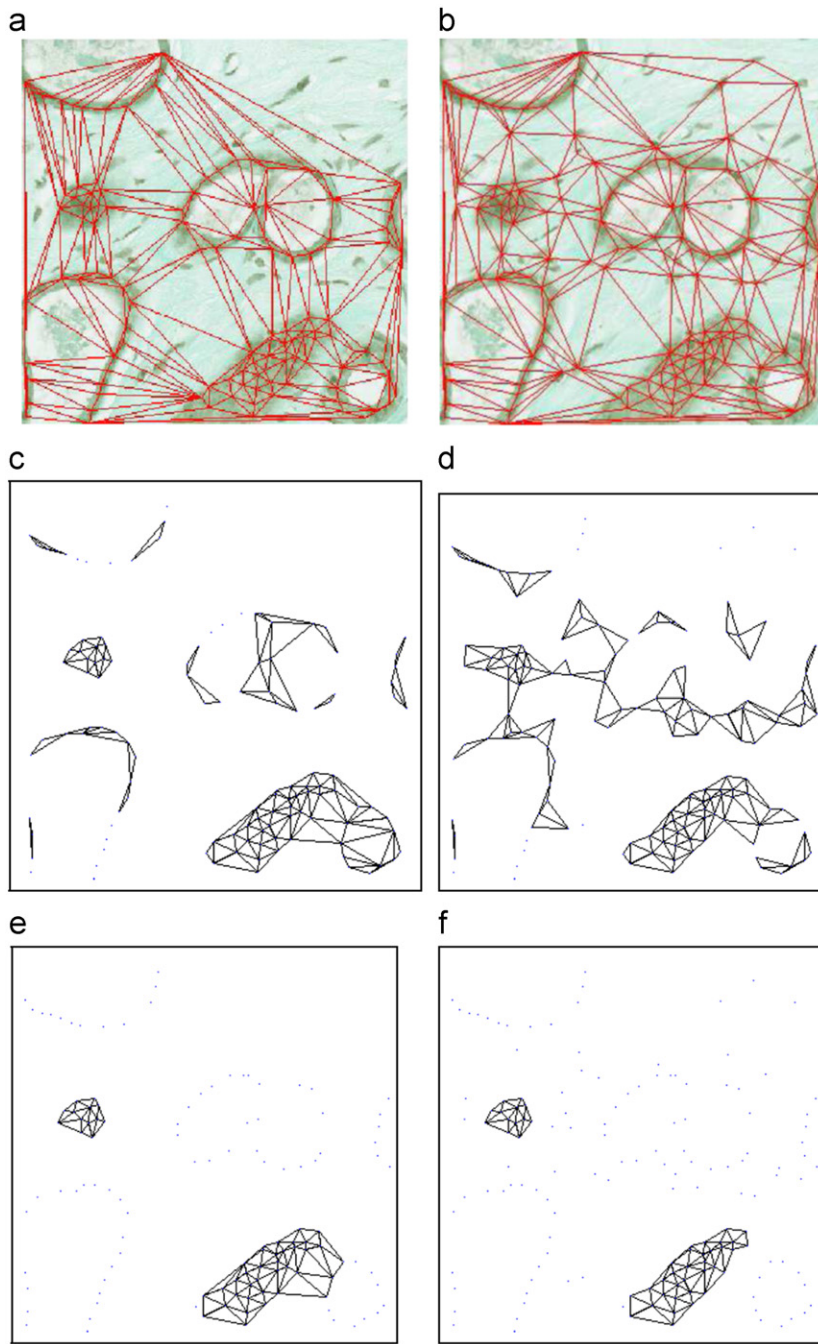


Fig. 23. (a) Point set extracted without artifact, M , and (b) with artifacts, M_{noise} ; (c) binarization of M ; (d) binarization of M_{noise} ; and (e) opening of M and (f) M_{noise} .

Acknowledgments

This study was partially supported by the French National Research Agency ANR, under reference ANR-10-TECS-015.

References

- [1] M. Zwicker, M. Pauly, O. Knoll, M. Gross, Pointshop 3D: an interactive system for point-based surface editing, in: SIGGRAPH, 2002.
- [2] H. Bunke, K. Riesen, Improving vector space embedding of graphs through feature selection algorithms, *Pattern Recognition* 44 (2011) 1928–1940.
- [3] F. Lafarge, G. Gimel'farb, X. Descombes, Geometric feature extraction by a multimarked point process, *IEEE Transactions on Pattern Analysis and Machine Intelligence* 32 (9) (2010) 1597–1609.
- [4] P.F. Felzenszwalb, R.B. Girshick, D. McAllester, D. Ramanan, Object detection with discriminatively trained part-based models, *IEEE Transactions on Pattern Analysis and Machine Intelligence* 32 (9) (2010) 1627–1645.
- [5] J. Shotton, A. Blake, R. Cipolla, Multi-scale categorical object recognition using contour fragments, *IEEE Transactions on Pattern Analysis and Machine Intelligence* 30 (7) (2008) 1270–1281.
- [6] V. Ferrari, L. Fevrier, F. Jurie, C. Schmid, Groups of adjacent contour segments for object detection, *IEEE Transactions on Pattern Analysis and Machine Intelligence* 30 (1) (2008) 36–51.
- [7] G. Erus, N. Lomenie, How to involve structural modeling for cartographic object recognition tasks in high-resolution satellite images? *Pattern Recognition Letters* 31 (10) (2010) 1109–1119.
- [8] K. Engel, K.D. Toennies, A. Brechmann, Part-based localisation and segmentation of landmark-related auditory cortical regions, *Pattern Recognition* 44 (2011) 2017–2033.
- [9] V.T. Ta, O. Lezoray, A. Elmoataz, S. Schupp, Graph-based tools for microscopic cellular image segmentation, pattern recognition, *Pattern Recognition* 42 (6)

- (2009) 1113–1125. (Special Issue on Digital Image Processing and Pattern Recognition Techniques for the Detection of Cancer).
- [10] S. Doyle, S. Agner, A. Madabhushi, M. Feldman, J. Tomaszewski, Automated grading of breast cancer histopathology using spectral clustering with textual and architectural image features, in: 5th IEEE International Symposium on Biomedical Imaging: From Nano to Macro, ISBI, 2008, pp. 496–499.
- [11] F. Meyer, Skeletons and perceptual graphs, *Signal Processing* 16 (4) (1989) 335–363.
- [12] Y. Liu, D. Zhang, G. Lu, W.-Y. Ma, A survey of content-based image retrieval with high-level semantics, *Pattern Recognition* 40 (1) (2007) 262–282.
- [13] M. Brown, G. Hua, S. Winder, Discriminative learning of local image descriptors, *IEEE Transactions on Pattern Analysis and Machine Intelligence* 33 (1) (2011) 43–57.
- [14] E. Clementini, P. Di Felice, Approximate topological relations, *International Journal of Approximate Reasoning* 16 (1997) 173–204.
- [15] S. Winter, Uncertain topological relations between imprecise regions, *International Journal of Geographical Information Science* 14 (5) (2000) 411–430.
- [16] P. Matsakis, L. Wendling, A new way to represent the relative position between real objects, *IEEE Transactions on Pattern Analysis and Machine Intelligence* 21 (7) (1999) 634–643.
- [17] Y. Cao, M. Ying, G. Chen, Retraction and generalized extension of computing with words, *IEEE Transactions on Fuzzy Systems* 15 (6) (2007) 1238–1250.
- [18] T.C. Havens, J.M. Keller, M. Popescu, Computing with words with the ontological self-organizing map, *IEEE Transactions on Fuzzy Systems* 18 (3) (2010) 473–485.
- [19] L.A. Zadeh, Fuzzy Logic=computing with words, *IEEE Transactions on Fuzzy Systems* 4 (1996) 103–111.
- [20] N. Lomenie, G. Stamon, Morphological mesh filtering and alpha-objects, *Pattern Recognition Letters* 29 (10) (2008) 1571–1579.
- [21] N. Lomenie, D. Racoceanu, Spatial relationships over sparse representations, in: *IEEE Image and Vision Computing*, Wellington, New Zealand, 2009.
- [22] S.C. Tan, K.M. Ting, S.W. Teng, A general stochastic clustering method for automatic cluster discovery, *Pattern Recognition* 44 (2011) 2786–2799.
- [23] L. Junlin, F. Hongguang, Molecular dynamics-like data clustering approach, *Pattern Recognition* 44 (2011) 1721–1737.
- [24] M. Tepper, P. Muse, A. Almansa, M. Mejail, Automatically finding clusters in normalized cuts, *Pattern Recognition* 44 (2011) 1372–1386.
- [25] N. Lomenie, G. Stamon, Point set analysis, in: P.W. Hawkes (Ed.), *Advances in Imaging and Electron Physics*, vol. 167, Academic Press, San Diego, 2011, pp. 255–294.
- [26] O. Colliot, O. Camara, I. Bloch, Integration of fuzzy spatial relations in deformable models—application to brain MRI segmentation, *Pattern Recognition* 8 (2006) 1401–1414.
- [27] D. Gianni, S. McKeever, T. Yu, R. Britten, H. Delingette, Sharing and reusing cardiovascular anatomical models over the web: a step towards the implementation of the virtual physiological human project, *Philosophical Transactions of the Royal Society A* 368 (2010) 3039–3056.
- [28] A. Mechouche, X. Morandi, C. Golbreich, B. Gibaud, A hybrid system using symbolic and numeric knowledge for the semantic annotation of sulco-gyral anatomy in brain MRI images, *IEEE Transactions on Medical Imaging* 28 (8) (2009) 1165–1178.
- [29] R. Swedlow, Nuclear dynamics: where genes are and how they got there, *Genome Biology* 2 (3) (2001).
- [30] I. Bloch, O. Colliot, R.M. Cesar, On the ternary spatial relation “between”, *IEEE Transactions on Systems Man and Cybernetics, Part B: Cybernetics* 36 (2) (2006) 312–327.
- [31] H. Edelsbrunner, D.G. Kirkpatrick, On the shape of set of points in the plane, *IEEE Transactions on Information Theory* 29 (1983) 551–559.
- [32] H. Edelsbrunner, E.P. Mücke, Three-dimensional alpha-shapes, *ACM Transactions on Graphics* 13 (1) (1994) 43–72.
- [33] H. Heijmans, C. Ronse, The algebraic basis of mathematical morphology I: dilations and erosions, *Computer Vision, Graphics, & Image Processing* 50 (3) (1990) 245–295.
- [34] J. Serra, *Image Analysis and Mathematical Morphology. Theoretical Advances*, vol. 2, London Academic Press, 1988.
- [35] M. Peternell, H. Pottmann, T. Steiner, *Hough Transform and Laguerre Geometry for the Recognition and Reconstruction of Special 3D Shapes*, Research Report, Institute of Discrete Mathematics and Geometry, Vienna, Austria, 2003.
- [36] H. Pottmann, T. Steiner, M. Hofer, C. Haider, A. Hanbury, The isophotic metric and its application to feature sensitive morphology, in: *European Conference on Computer Vision (ECCV'04)*, Lecture Notes in Computer Sciences, vol. 3024, Springer, 2004, pp. 560–572.
- [37] H. Heijmans, P. Nacken, A. Toet, L. Vincent, Graph morphology, *Journal of Visual Communication and Image Representation* 3 (1) (1992) 24–38.
- [38] J. Roerdink, Mathematical morphology on the sphere, in: *SPIE Conference on Visual Communications and Image Processing*, 1990, pp. 263–271.
- [39] J. Roerdink, Manifold shape: from differential geometry to mathematical morphology, in: *Shape in Picture*, Springer-Verlag, 1994.
- [40] C. Rossel, L. Kobelt, H.P. Seidel, Extraction of feature lines on triangulated surfaces using morphological operators, in: *Smart Graphics, AAAI Spring Symposium*, 2000.
- [41] L. Vincent, Graphs and mathematical morphology, *Signal Processing* 16 (4) (1989) 365–388.
- [42] I. Bloch, H. Maitre, Fuzzy mathematical morphologies: a comparative study, *Pattern Recognition* 28 (9) (1995) 1341–1387.
- [43] J. Chaussard, M. Couprise, H. Talbot, Robust skeletonization using the discrete lambda-medial axis, *Pattern Recognition Letters* (2010). doi:10.1016/j.patrec.2010.09.002.
- [44] D. Dubois, H. Prade, *Fuzzy Sets and Systems: Theory and Applications*, Academic, New York, 1980.
- [45] V. Della Mea, C. Beltrami, Analysis of the spatial arrangement of cells in the proliferative breast lesions, in: *Image Analysis and Processing, Lecture Notes in Computer Science*, vol. 974, 1995, pp. 247–252.
- [46] V. Della Mea, N. Finato, C. Beltrami, A graph-based approach to the structural analysis of proliferative breast lesions, in: *Artificial Intelligence in Medicine, Lecture Notes in Computer Science*, vol. 934, 1995, pp. 413–414.
- [47] C. Huang, A. Veillard, L. Roux, N. Lomenie, D. Racoceanu, Time-efficient sparse analysis of histopathological whole slide images, *Computerized Medical Imaging and Graphics* 35 (7) (2011) 579–591.
- [48] J. Cousty, L. Najman, J. Serra, Some morphological operators in graph spaces, in: *Mathematical Morphology and its Application to Signal and Image Processing, Lecture Notes in Computer Sciences*, vol. 5720, Springer, 2009, pp. 149–160.
- [49] R. Levillain, T. Géraud, L. Najman, Milena: write generic morphological algorithms once, in: *Mathematical Morphology and its Application to Signal and Image Processing, Lecture Notes in Computer Sciences*, vol. 5720, Springer, 2009, pp. 295–306.

Nicolas Loménie is an associate professor at University Paris Descartes and a research fellow at IPAL (joint NUS/I2R/CNRS lab) in Singapore since 2009. His research interests include image analysis, pattern recognition and computer vision. He has worked so far on object recognition issues in VHR satellite images, medical image screening and stereoscopic point set analysis. Since 2009, his current research topics include knowledge-driven medical image analysis, in particular for the exploration of huge histopathological images.

Daniel Racoceanu received M.Eng. degree in mechatronics from the Politehnica University of Timisoara in 1992, M.Sc. degree in automatics and industrial informatics from the University of Technology of Belfort-Montbéliard (UTBM), France in 1993, Ph.D. degree in 1997 and Habil-Dr. degree in 2006 in control and computer sciences from the University of Besançon, France. He was a project manager at General Electric Energy Products – Europe, Belfort, France, before joining, in 1999 a chair of associate professor at the Faculty of Sciences of the University of Besançon, France, where he courses until 2005 in the field of artificial intelligence, computer vision, industrial informatics, automation, control science and production systems. He is a senior scientist at the French National Research Center (CNRS); he is the director (France) of Image & Pervasive Access Lab (IPAL), the International Joint Research Unit (UMI CNRS 2955) created in Singapore between the CNRS, the National University of Singapore (NUS), the Institute for Infocomm Research (I2R) of the Singaporean Agency for Science, Technology and Research A*STAR and the University Joseph Fourier of Grenoble, France (UJF). From 1999 to 2005, He was with FEMTO-ST/AS2M Lab of Besançon, France, working in diagnosis/prognosis area using artificial intelligent techniques (Dynamic Neural Networks; Fuzzy Logic, Neuro-Fuzzy Systems). His actual researches in IPAL focus on intelligent diagnosis/prognosis assistance using medical image and knowledge-based reasoning systems, content and context based medical image retrieval and medical multimedia fusion.